Reduction of $CoMoO_4$ and $NiMoO_4$: *in situ* time-resolved XRD studies

José A. Rodriguez [a,*], Jae Y. Kim [a], Jonathan C. Hanson [a], and Joaquín L. Brito [b]

[a] *Chemistry Department, Brookhaven National Laboratory, Upton, NY 11973, USA*
[b] *Centro de Química, Instituto Venezolano de Investigaciones Científicas (IVIC), Apartado 21827, Caracas 1020-A, Venezuela*

Received 14 February 2002; accepted 23 April 2002

One method frequently employed for the preparation of active oxide catalysts consists of partial reduction under hydrogen at elevated temperatures. In this process, it is important to identify well-defined suboxides that can have high catalytic activity and are stable at the elevated temperatures typical of many catalytic reactions. Our results for the reaction of H_2 with α-$NiMoO_4$ and β-$CoMoO_4$ show that *in situ* time-resolved X-ray diffraction is a powerful technique to study the reduction/activation of mixed-metal oxides. It is clearly shown that the mechanism for the reduction of a mixed-metal oxide catalyst can exhibit drastic changes with respect to that observed for simple metal oxide catalysts. The generation of stable suboxides is difficult to predict. Thus, the reaction of H_2 with α-$NiMoO_4$ does not lead to formation of a well-ordered $NiMoO_x$ intermediate. On the other hand, during the reduction of β-$CoMoO_4$, $Co_2Mo_3O_8$ and/or $CoMoO_3$ are formed. These chemical transformations are accompanied by changes in the line shape and position of the Mo L_{II}-edge in XANES and affect the behavior of reduced $NiMoO_4$ and $CoMoO_4$ catalysts. Induction times were detected in the reduction process of $CoMoO_4$. From the present results and data previously reported for NiO, it is clear that this phenomenon should be taken into consideration when aiming at the activation of oxide catalysts via reduction in H_2.

KEY WORDS: catalyst activation; oxides; molybdates; hydrogen; X-ray diffraction; X-ray absorption spectroscopy.

1. Introduction

Metal oxides are used as catalysts in a large variety of industrial processes that involve the activation or conversion of hydrocarbons [1,2]. In most cases, pure stoichiometric oxides do not exhibit high catalytic activity [2]. One method frequently employed for the preparation of active oxide catalysts consists of reduction under hydrogen at elevated temperatures [2,3]. In this respect, it is important to develop techniques for *in situ* characterization since different kinetic models have been proposed for the reduction of oxides [2,3] and, in general, the molecular or atomic steps in the reduction process are poorly understood [2,4]. Recently, time-resolved X-ray diffraction (XRD) has been used to study the reduction of MoO_3 [5] and NiO [6] *in situ* under atmospheric pressures. The combination of the high intensity of synchrotron radiation with new data-collection devices makes it possible to conduct subminute, time-resolved XRD experiments under a wide variety of temperature and pressure conditions ($-190\,^{\circ}C < T > 900\,^{\circ}C$; $P < 45$ atm) [7]. For the reaction of H_2 with MoO_3 and NiO, time-resolved XRD has shown the existence of well-defined intermediates (suboxides) and allowed the identification of key steps in the reduction process [5,6]. Substantial differences have been found in the reaction mechanisms for the reduction of MoO_3 and NiO [5,6]. They highlight the need for systematic studies on this type of chemical transformation. An important open question is how a mixed-metal oxide will behave at different stages of the reduction/activation process [2,3,8,9]. In principle, the presence of two metals in the system can lead to the formation of novel suboxides during the reduction which could have a superior performance in catalytic applications [1,2]. In this work, we investigate the reduction of $CoMoO_4$ and $NiMoO_4$ with H_2 using *in situ* time-resolved XRD and X-ray absorption near-edge spectroscopy (XANES).

Cobalt and nickel molybdates ($AMoO_4$, A = Co or Ni) are important components of commercial catalysts for the partial oxidation of hydrocarbons [1,8] and precursors in the synthesis of hydrodesulfurization (HDS) catalysts [9]. The $AMoO_4$ compounds are ideal for exploring possible correlations among the structural, electronic and chemical properties of mixed-metal oxide catalysts [9–12], a subject that is receiving a lot of attention [8,9,13,14]. In general, these molybdates can be seen as the product of adding CoO or NiO to MoO_3, but here we observe a distinctive behavior during the reduction of $CoMoO_4$ or $NiMoO_4$. Our results show that *in situ* time-resolved X-ray diffraction is a powerful technique for monitoring the reduction/activation of mixed-metal oxide catalysts.

2. Experimental

α-$NiMoO_4$ and β-$CoMoO_4$ were prepared by heating the corresponding $AMoO_4 \cdot nH_2O$ hydrates as described

* To whom correspondence should be addressed.

1011-372X/02/0900-0103

in the literature [9]. High-purity (>99.9%) powders of NiO, CoO and MoO_3 were acquired from commercial sources. The time-resolved XRD data were collected on beam line X7B of the National Synchrotron Light Source (NSLS) [7]. Samples of the molybdates were loaded in an open sapphire capillary attached to a flow-reaction cell similar to those described in refs. [16,17]. The capillary was connected to 1/16 in. Swagelok style fittings with Vespel ferrules. A 0.010 in. chromel-alumel thermocouple was inserted straight into the capillary near the oxide sample [16]. The oxide sample was heated using a small resistance heater wrapped around the capillary. Diffraction patterns ($\lambda = 0.9276$ or 0.9034 Å) were recorded at temperatures in the range 200–900 °C under a 5% H_2–95% He gas mixture (flow rate ~15–20 cm^3/min) using a MAR345 detector. The typical time required for collecting an individual diffraction pattern was in the range of 1–3 min. The powder rings were integrated using the FIT2D code [18]. Rietveld refinements were performed with the program GSAS [19].

The Mo L_{II}-edge XANES spectra were recorded at the NSLS on beam line X19A in the "fluorescence-yield mode" using a modified Stern–Heald–Lytle cell. The energy resolution was ~0.5 eV. In these experiments the oxide samples were exposed to a 5% H_2–95% He gas current at several temperatures, followed by evacuation of the gas and sealing of the reaction cell before taking the XANES data at ~25 °C.

3. Results and discussion

We will begin by examining XRD results for the reduction in H_2 of simple oxides (CoO, NiO and MoO_3), before dealing with the reduction of α-$NiMoO_4$ and β-$CoMoO_4$. Figure 1(a) shows a series of diffraction patterns obtained during the temperature-programmed reduction of a MoO_3 powder. The XRD data were recorded while the temperature was ramped from 25 to 725 °C at a rate of 5.8 °C/min. Figure 1(b) shows the intensities of the indicated XRD signals of several Mo oxides as a function of sample temperature. Our results are in good agreement with those previously reported in refs. [5,10]. The onset for the reduction of MoO_3 is observed near 400 °C, and Mo_4O_{11} and MoO_2 are produced as intermediates before metallic molybdenum appears at very high temperature [10]. By 600 °C, Mo_4O_{11} is the dominant species in the sample. The formation of Mo_4O_{11} as a suboxide during the reduction of MoO_3 has been found in other works [5,20,21]. In fact, a large series of different Mo_xO_y suboxides exists between MoO_3 and MoO_2 [21b,c], due to the flexibility of the basic structure of MoO_3 that makes possible the formation of so-called shear planes by rearrangement of the MoO_6 octahedra from corner-linked to edge-linked after ordered arrays of oxygen vacancies are removed [21d]. However, such shear structures are not thermodynamically stable under usual TPR conditions [21e] and so are rather difficult to detect. Thus, under more severe reduction conditions (>40 vol% hydrogen) no accumulation of Mo_4O_{11} was seen (i.e., $MoO_3 \rightarrow MoO_2 \rightarrow Mo$).

Time-resolved XRD data for the reduction of NiO are displayed in figure 2. In this case, the oxide → metal transformation occurs at temperatures (<450 °C) much lower than those seen for MoO_3, a trend which is also observed in experiments of H_2-TPR that use a different heating rate [6,10]. In the case of NiO, the XRD results show a direct NiO → Ni transformation and no suboxide

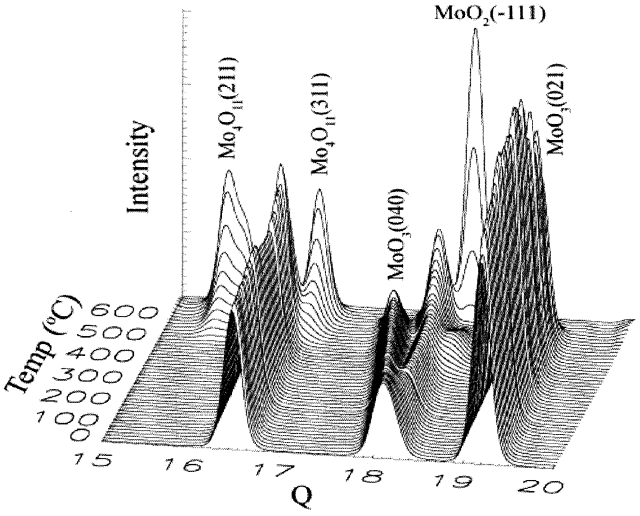

(a)

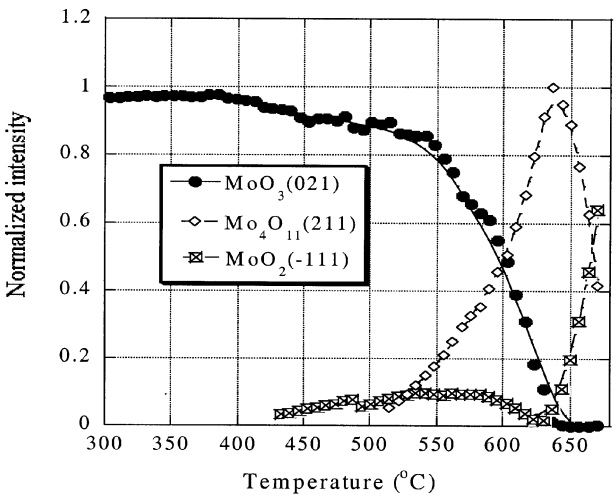

(b)

Figure 1. (a) Time-resolved X-ray diffraction patterns ($\lambda = 0.9276$ Å) acquired during the heating (5.8 °C/min) of a MoO_3 powder from 25 to 725 °C under a flow of 5% H_2–95% He. Q is in inverse nanometer units. (b) Integrated intensity (normalized to the individual maxima) for diffraction lines of MoO_3, Mo_4O_{11} and MoO_2 as a function of sample temperature. The solid curves are for guiding the eye.

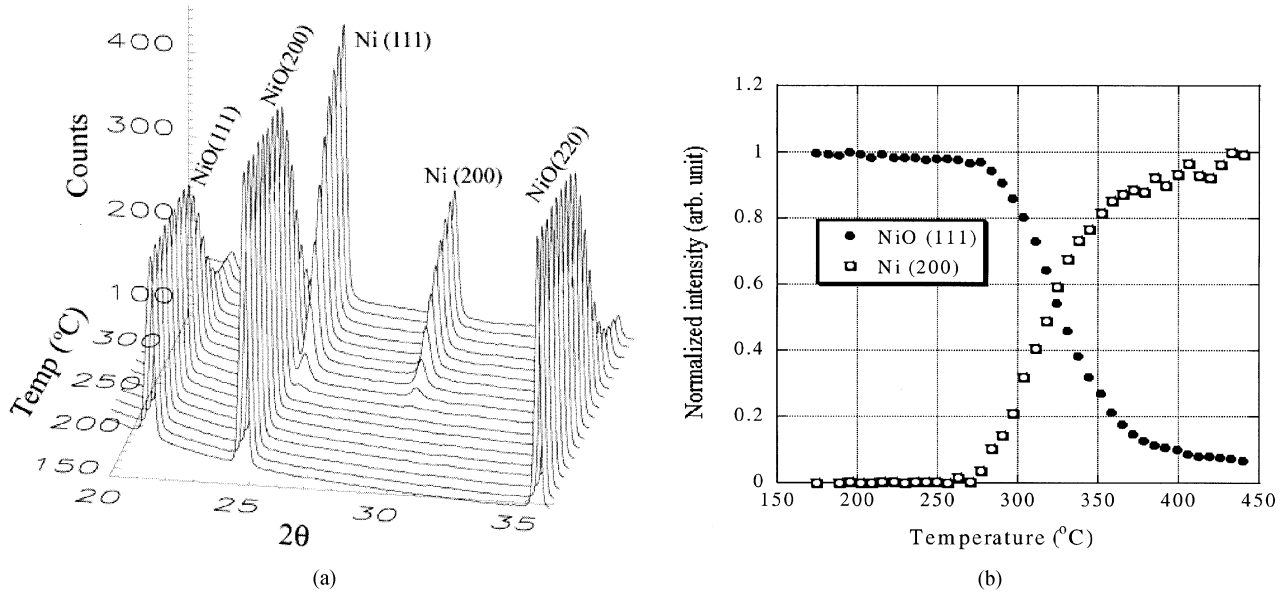

Figure 2 (a) Time-resolved X-ray diffraction patterns ($\lambda = 0.9034$ Å) acquired during the heating (5.8 °C/min) of a NiO powder from 25 to 725 °C under a flow of 5% H_2–95% He. (b) Integrated intensity for diffraction lines of NiO and Ni as a function of sample temperature.

(NiO_x) is accumulated as an intermediate. An identical fact was observed when the reduction of NiO was performed under isothermal conditions at temperatures in the range 270–300 °C. This observation (absence of a NiO_x suboxide) is consistent with results of XANES/EXAFS measurements for the H_2/NiO system [6]. When CoO was reduced under the same experimental conditions as figure 2, a complete $CoO \rightarrow Co$ transformation occurred between 200 and 400 °C, again without accumulation of an intermediate. In the case of MoO_3, the existence of several oxidation states for the cations (+6 to 0), the open and flexible structure of the trioxide, and the slow rate of reduction, all favor the generation of suboxides during the reduction process. On the other hand, no suboxide between MoO_2 and metallic Mo has been confirmed [5,21e].

It is important to examine the reduction of α-$NiMoO_4$, since this mixed-metal oxide in essence is a combination of NiO and MoO_3. In the α-$NiMoO_4$ compound the Ni and Mo atoms are in an octahedral coordination [11] as in NiO and MoO_3. There are some differences in the Ni–O and Mo–O bond lengths [11], but the oxidation states of the metal atoms in the mixed-metal oxide are essentially Ni(+2) and Mo(+6) as in the pure oxides [11,22]. The behavior of α-$NiMoO_4$ during reduction is interesting since several compounds of the $AMoO_x$ type that have a content of oxygen smaller than in an $AMoO_4$ oxide are known [10,23,24]. Figure 3 shows time-resolved XRD data for the reaction of α-$NiMoO_4$ with hydrogen. Near 350 °C the diffraction lines for the α-$NiMoO_4$ compound begin to disappear without the appearance of new lines for $Ni_2Mo_3O_8$ or $NiMoO_x$ species in general [10,23,24]. At 500 °C a diffraction pattern is observed which could be approximately fitted by a combination of Ni_4Mo, Ni and NiO [25]. However, a much better fit is obtained by an unreported compound with tetragonal lattice ($a = 5.065$ Å and $b = 6.800$ Å). Additional reduction leads to the appearance of diffraction lines for metallic Mo and Ni above 600 °C. During the reduction process intense features developed at low order in 2θ (<5°, not shown) suggesting the formation of nanoparticles. Experiments were also carried out for the isothermal reduction of α-$NiMoO_4$ as shown in figure 4. Again, no well-defined $NiMoO_x$ intermediate or suboxide was detected. The Ni atoms in α-$NiMoO_4$ facilitate the reduction process with respect to MoO_3 (compare reaction temperatures in figures 1(b) and 3(b)), and this transformation is probably too fast for allowing the generation of an ordered $NiMoO_x$ suboxide. Similarly, for the heating of heavily reduced α-$NiMoO_4$ in O_2, the full reoxidation and formation of $NiMoO_4$ occurs near 400 °C without the appearance of an ordered $NiMoO_x$ intermediate [26].

The isothermal data in figure 4 allow a more detailed study of the reduction kinetics of α-$NiMoO_4$ than the temperature ramp in figure 3. For a temperature of 325 °C, the reduction rate is relatively slow and no full conversion of $NiMoO_4$ is seen after 500 min under hydrogen. In general, the line shape of the intensity *versus* time curves near $t = 0$ does not point to an autocatalytic process [2]. Such a behavior is consistent with a reduction process that follows the so-called "contracting-sphere model" [2]. According to this model the reduction process involves the rapid formation of a uniform layer of reduced oxide around the sample. The thickness of this reduced layer grows uniformly, resulting in a spherical core of oxide that shrinks with

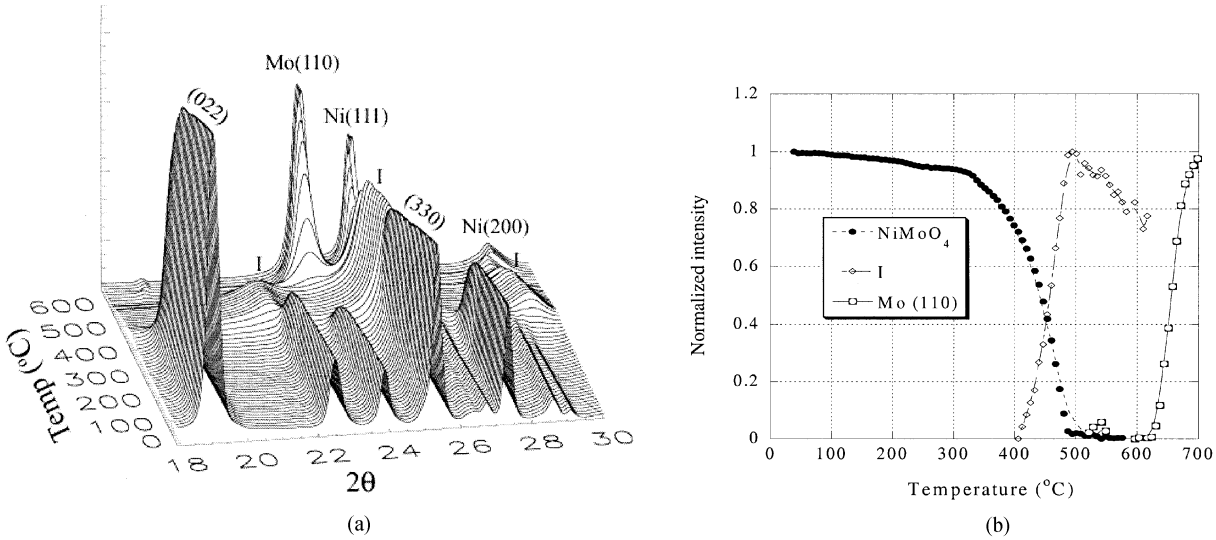

Figure 3. (a) Time-resolved X-ray diffraction patterns ($\lambda = 0.9034$ Å) recorded during the heating (5.8 °C/min) of a α-$NiMoO_4$ powder from 25 to 725 °C under a flow of 5% H_2–95% He. The intermediate phase is denoted as "I". (b) Integrated intensity for diffraction lines of α-$NiMoO_4$, "I", and Mo as a function of sample temperature.

time [2]. The rate of reaction is dominated by the diffusion of ions and reductant across the interface between the oxide and the reduced layer [2].

XANES has proven to be very useful for monitoring the reduction of MoO_3 [5] and NiO [6]. Usually, the technique is sensitive to changes in the oxidation state of transition metal atoms [27]. Figure 5 shows Mo L_{II}-edge XANES spectra for the reduction of α-$NiMoO_4$. After exposure of α-$NiMoO_4$ to hydrogen up to 600 °C, one sees a substantial change in the line shape of the Mo L_{II}-edge XANES spectrum. However, most of the molybdenum features still appear at photon energies very different from those seen for metallic Mo, which is consistent with the fact that the dominant molybdenum species in the sample at this reduction stage is amorphous MoO_2 [9,10,25]. Further hydrogen exposure to 725 °C produces a shift in the Mo L_{II}-edge features toward the position of the corresponding metallic Mo features. At this point, the system probably contains a mixture of Mo and a Ni/Mo alloy plus a minor amount of MoO_2 instead of α-$NiMoO_4$, as shown by XRD studies (see figure 3).

In β-$CoMoO_4$, Co is in an octahedral environment, whereas Mo is in a pseudo-tetrahedral (or highly distorted octahedral) coordination [11,12,24,26]. For the reduction of β-$CoMoO_4$, the experiments of time-resolved XRD showed the presence of well-ordered oxide intermediates. Figure 6(a) displays diffraction patterns acquired during the heating of β-$CoMoO_4$ in a 5% H_2–95% He stream. Near 500 °C the diffraction

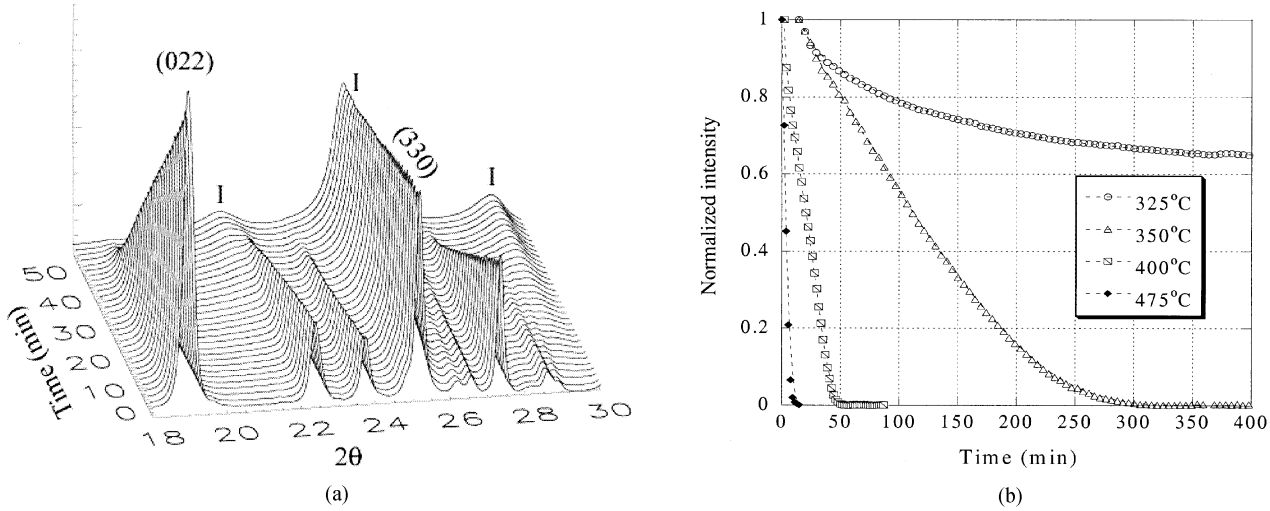

Figure 4. (a) Time-resolved XRD data ($\lambda = 0.9034$ Å) for the isothermal reduction of α-$NiMoO_4$ at 400 °C. The intermediate phase is denoted as "I". (b) Change of integrated intensity for the isothermal reduction of α-$NiMoO_4$, (022) line, at different temperatures as a function of time. The traces connecting the points in the graph are drawn to guide the eye.

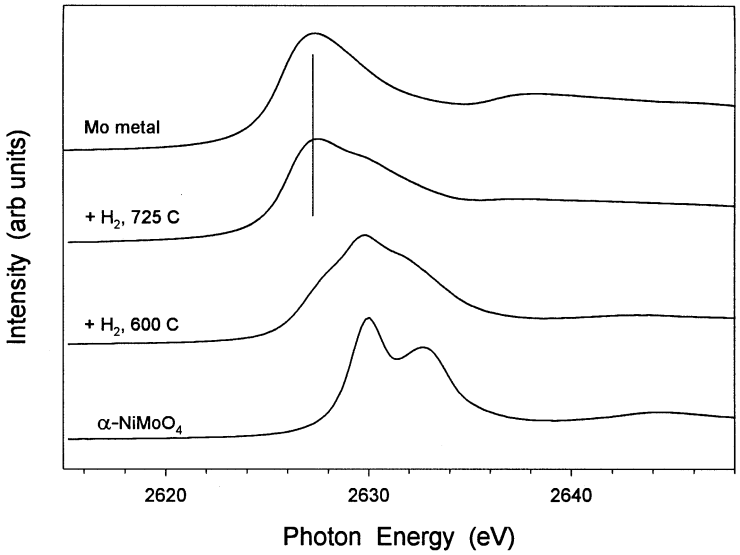

Figure 5. Mo L_{II}-edge XANES data for the reduction of α-$NiMoO_4$. The sample was heated to the indicated temperatures, and the spectra recorded after exposure of the sample to a 5% H_2–95% He mixture.

lines for β-$CoMoO_4$ disappear and a completely different diffraction pattern appears that contains lines for $Co_2Mo_3O_8$ [24b] or $CoMoO_3$ [28] and CoO [29]. It should be pointed out that $CoMoO_3$ [28] has similar cell dimensions to $Co_2Mo_3O_8$ [24b] and it is difficult to distinguish them when using X-ray powder diffraction.

For the reaction of β-$CoMoO_4$ with H_2, the relative amount of $CoMoO_3$ and $Co_2Mo_3O_8$ formed depended on the heating rate. The formation of $Co_2Mo_3O_8$/$CoMoO_3$ as a suboxide during the reduction of β-$CoMoO_4$ was more dominant when the reaction was carried out under isothermal conditions (for example, see figure 7). The reduction of β-$CoMoO_4$ occurred at lower temperatures than the reduction of MoO_3, but higher than the reduction of α-$NiMoO_4$. This trend suggests that the relatively rapid reduction of α-$NiMoO_4$ probably prevents the formation of an ordered $NiMoO_x$ intermediate. We also investigated the reduction of the β phase of $NiMoO_4$. Experiments of H_2-TPR indicate that in this system the consumption of hydrogen occurs at a lower temperature than in α-$NiMoO_4$ [9,10], and the fast reduction of the oxide once again results in no production of a $NiMoO_x$ suboxide in time-resolved XRD.

Figure 7a displays time-resolved XRD data for the reduction of β-$CoMoO_4$ under isothermal conditions. Clearly, there is an induction period for the reduction of the oxide. In all cases, the reaction is initially slow, and then the reduction rate accelerates in a way consistent with an autocatalytic process. The magnitude of

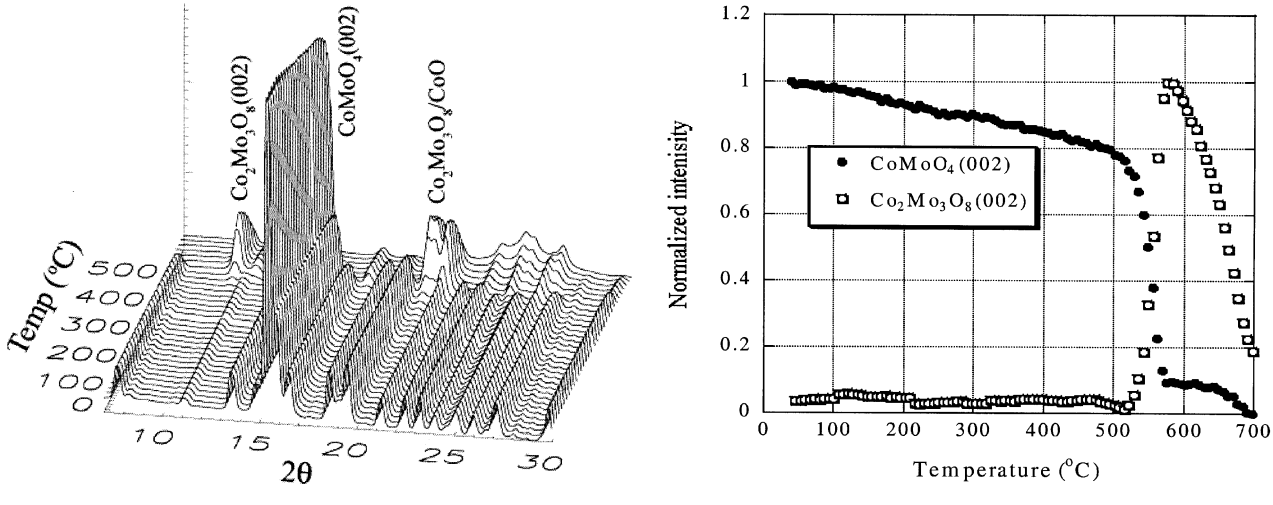

Figure 6. (a) Time-resolved X-ray diffraction patterns ($\lambda = 0.9034$ Å) acquired during the heating (5.8 °C/min) of a β-$CoMoO_4$ powder from 25 to 725 °C under a flow of 5% H_2–95% He. (b) Integrated intensity for β-$CoMoO_4$ and $Co_2Mo_3O_8$ (or $CoMoO_3$) diffraction lines as a function of sample temperature.

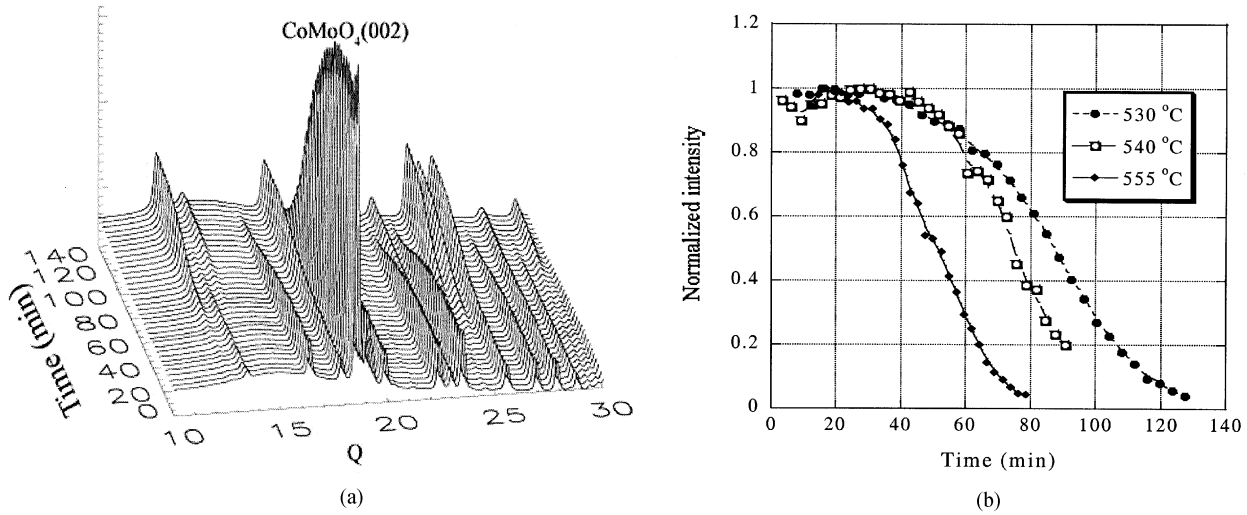

Figure 7. (a) Time-resolved XRD data for the isothermal reduction of β-$CoMoO_4$ measured at 530 °C. (b) Change of intensity for $CoMoO_4$(002) as a function of time for different temperatures. The solid curves are for guiding the eye.

the induction time decreases when the temperature of the sample increases. Depending on the preparation of the sample (i.e., amount of defect sites), an induction time has also been observed for the reduction of NiO [6]. Different kinetic models have been proposed to explain this phenomenon [2,3,6]. It could be associated with the production of sites on the oxide surface with a high efficiency for the adsorption and dissociation of H_2 [6,30,31]. The removal of oxygen from the bulk or the nucleation of the metal phase probably become rate-limiting factors when a substantial amount of H is available on the oxide surface. The data in figures 4 and 7 show different kinetics for the reduction of the mixed-metal oxides. The surface area of the α-$NiMoO_4$ sample, $38\,m^2\,g^{-1}$ [9], was almost double that of the β-$CoMoO_4$ sample, $20\,m^2\,g^{-1}$ [9]. Thus, it is likely that the amount of defects and imperfections in the α-$NiMoO_4$ system was larger than in the β-$CoMoO_4$ system [9], making possible the direct reduction of the nickel molybdate without the need for an induction time. Large concentrations of defect sites suppress the need for an induction time in NiO [6].

The results described above point to large variations in the reduction pathways for NiO, CoO, MoO_3, $NiMoO_4$ and $CoMoO_4$. The behavior seen during the reduction of the mixed-metal oxides is not the product of adding trends found for the monometallic oxides ($NiO + MoO_3$ or $CoO + MoO_3$). In particular, the generation of stable suboxides is difficult to predict. Thus, it is really necessary to monitor the evolution of the sample *in situ* when a mixed-metal oxide catalyst is activated by reduction in H_2. Time-resolved XRD can be utilized to accomplish this task.

Cobalt and nickel molybdates are used as catalysts in the transformation of hydrocarbons [1,2,8] and precursors in the synthesis of HDS catalysts [9]. Our results indicate that well-defined suboxides can be expected after activating $CoMoO_4$ in H_2. This is not the case for $NiMoO_4$. For the preparation of active HDS catalysts, $CoMoO_4$ and $NiMoO_4$ are pretreated in mixtures of H_2/H_2S, molybdate $+ H_2/H_2S \rightarrow$ metal sulfide + water, with the hydrogen helping in the removal of the oxygen from the oxides [9]. The sulfidation of these mixed-metal oxides is faster than for MoO_3 [9,10]. This difference can originate in the fact that it is easier to remove oxygen from $CoMoO_4$ or $NiMoO_4$ than from MoO_3, as seen by comparing figures 1 and 3 or 6. Also, the existence of Co and Ni cations in the mixed-metal oxides, adsorption sites which have special electronic properties with respect to Mo cations [11,26], could facilitate interactions with H_2 and H_2S. The reaction of H_2 with $NiMoO_4$ produces an amorphous system (figure 3) that upon full sulfidation gives disordered $NiMoS_x$ catalysts [32] with very high activity for HDS reactions [9,32].

4. Conclusions

In situ time-resolved XRD is a useful technique to study the reduction (or activation) of mixed-metal oxide catalysts. It allows the identification of intermediates and products and can be employed to monitor the kinetics of the reduction process. The XRD results discussed above clearly show that the mechanism for the reduction of a mixed-metal oxide catalyst can exhibit drastic changes with respect to those observed for the corresponding single-metal oxide catalysts. The generation of stable suboxides is difficult to predict. Thus, the reaction of H_2 with α-$NiMoO_4$ or β-$NiMoO_4$ does not lead to formation of a well-ordered $NiMoO_x$ intermediate. On the other hand, during the reduction of β-$CoMoO_4$, $Co_2Mo_3O_8$ and/or $CoMoO_3$ are formed. These chemical transformations are accompanied by changes in the line

shape and position of the Mo L_{II}-edge in XANES. Induction times were detected in the reduction process of β-$CoMoO_4$. From the present results, and data previously reported for NiO [6], it is clear that this phenomenon should be taken into consideration when aiming at the activation of oxide catalysts via reduction in H_2.

Acknowledgment

The research carried out at the Chemistry Department of Brookhaven National Laboratory was financed through contract DE-AC02-98CH10086 with the US Department of Energy (Division of Chemical Sciences). The NSLS is supported by the Divisions of Materials and Chemical Sciences of DOE.

References

[1] J.M. Thomas and W.J. Thomas, *Principles and Practice of Heterogeneous Catalysis* (VCH, New York, 1997).
[2] H.H. Kung, *Transition Metal Oxides: Surface Chemistry and Catalysis* (Elsevier, New York, 1989).
[3] B. Delmon in: *Handbook of Heterogeneous Catalysis*, eds. G. Ertl, H. Knözinger and J. Weitkamp (VCH-Wiley, New York, 1997) p. 264.
[4] V.E. Henrich and P.A. Cox, *The Surface Science of Oxides* (Cambridge University Press, Cambridge, UK, 1994).
[5] T. Ressler, R.E. Jentoft, J. Wienold, M.M. Günter and O. Timpe, J. Phys. Chem. B 104 (2000) 6360.
[6] J.A. Rodriguez, J.C. Hanson, A. Frenkel, J.-Y. Kim and M. Perez, J. Am. Chem. Soc. 124 (2002) 346.
[7] P. Norby and J. Hanson, Catal. Today 39 (1998) 301 and references therein.
[8] (a) J. Zou and G.L. Schrader, J. Catal. 161 (1996) 667; (b) J. Miller, A.G. Sault, N.B. Jackson, L. Evans and M.M. Gonzales, Catal. Lett. 58 (1999) 147.
[9] J.L. Brito and A.L. Barbosa, J. Catal. 171 (1997) 467 and references therein.
[10] J.L. Brito, J. Laine and K.C. Pratt, J. Mater. Sci. 24 (1989) 425.
[11] J.A. Rodriguez, J.C. Hanson, S. Chaturvedi, A. Maiti and J.L. Brito, J. Chem. Phys. 112 (2000) 935.
[12] J.A. Rodriguez, J.C. Hanson, S. Chaturvedi, A. Maiti and J.L. Brito, J. Phys. Chem. B 104 (2000) 8145.
[13] N.M. Rodriguez, S.L. Soled and J. Hrbek, eds, *Recent Advances in Catalytic Materials*, MRS Symposium Proceedings, Vol. 497 (Materials Research Society, Pittsburgh, PA, 1998).
[14] Symposium on the Characterization of Mixed-Metal Oxide Catalysts, 215th National Meeting of the American Chemical Society, Dallas, TX, March–April 1998.
[16] P.J. Chupas, M.F. Ciraolo, J.C. Hanson and C.P. Grey, J. Am. Chem. Soc. 123 (2001) 1694.
[17] B.S. Clausen, G. Steffensen, B. Fabius, J. Villadsen, R. Freidenhans and H. Topsoe, J. Catal. 132 (1991) 524.
[18] A.P. Hammersely, S.O. Svensson and A. Thompson, Nucl. Instrum. Meth. Phys. Res. 346 (1994) 321.
[19] A.C. Larson and R.B. von Dreele, GSAS—General Structure Analysis System, Report LAUR 86-748, Los Alamos National Laboratory, Los Alamos, NM, 1995.
[20] R. Burch, J. Chem. Soc., Faraday Trans. I 74 (1978) 2982.
[21] (a) J. Sloczynski and W. Bobinski, J. Solid State Chem. 92 (1991) 420; (b) A. Ueno, Y. Kotera, S. Okuda and C.O. Bennet, in: *Proceedings of the 4th International Conference on the Chemistry and Uses of Molybdenum*, eds. H.F. Barry and P.C.H. Mitchell (Climax Molybdenum Co., Ann Arbor, 1982), p. 250; (c) L. Kihlborg, Archiv. Kemi. 21 (1963) 443; (d) J. Haber in: *Proceedings of the 2nd International Conference on the Chemistry and Uses of Molybdenum*, ed. P.C.H. Mitchell (Climax Molybdenum Co., London, 1977), p. 119; (e) P. Arnoldy, J.C.M. de Jonge and J.A. Moulijn, J. Phys. Chem. 89 (1985) 4517.
[22] J.A. Rodriguez, S. Chaturvedi, J.C. Hanson, A. Albornoz and J.L. Brito, J. Phys. Chem. B 102 (1998) 1347.
[23] L.M. Madeira, M.F. Portela, C. Mazzochia, A. Kaddouri and R. Anouchinsky, Catal. Today 40 (1998) 229.
[24] (a) J. Haber and J. Janas, in: *Reaction Kinetics in Heterogeneous Chemical Systems*, ed. P. Barret (Elsevier, Amsterdam, 1975), p. 737; (b) W.H. McCarroll, L. Katz and R. Ward, J. Am. Chem. Soc. 79 (1966) 5410.
[25] JCPDS Powder Diffraction File No. 4-850. International Centre for Diffraction Data, Swarthmore, PA 1989; PDF No 3-1036; PDF No 4-850; PDF No 44-1159.
[26] J.A. Rodriguez, S. Chaturvedi, J.C. Hanson and J.L. Brito, J. Phys. Chem. B 103 (1999) 770.
[27] J.G. Chen, Surf. Sci. Reports 30 (1997) 1.
[28] P. Bautry, P. Courty, J.-C. Daumas and R. Montarnal, Bull. Soc. Chim. France (1968) 4050.
[29] PDF No 43-1004.
[30] R.P. Furstenau, G. McDougall and M.A. Langell, Surf. Sci. 150 (1985) 55.
[31] J.G. Chen, D.A. Fischer, J.H. Hardenbergh and R.B. Hall, Surf. Sci. 279 (1992) 13.
[32] J.L. Brito, A.L. Barbosa, A. Albornoz, F. Severino and J. Laine, Catal. Lett. 26 (1994) 329.